CHEMISTRY OF MATERIALS

Open Access

pubs.acs.org/cm

Article

Silyl Hot-Injection Versus Thiocyanate Heat-Up Synthesis of Chalcohalides: Pushing the Size and Composition Envelope

Published as part of Chemistry of Materials special issue "Honoring the Outstanding Contributions of Mercouri Kanatzidis to Chemistry of Materials".

Eve K. Stegner,[‖] Md Riad Sarkar Pavel,[‖] Anuluxan Santhiran, Jack Lawton, Juan-Pablo Correa-Baena, Aaron J. Rossini, and Javier Vela*

Cite This: *Chem. Mater.* 2026, 38, 2755−2766

Read Online

ACCESS | Metrics & More | Article Recommendations | Supporting Information

ABSTRACT: Chalcohalide semiconductors are rapidly gaining traction as stable, biocompatible materials for energy conversion applications. While the solid-state synthesis of bulk chalcohalides is relatively well-developed, the colloidal chemistry of these materials is still in its early stages. Colloidal semiconductors are often advantageous in device fabrication due to the cost effectiveness of solution processing. Thus, we aim to increase the utility of chalcohalides in device fabrication by establishing solution phase chemistry of promising compositions. We show that silyl hot-injection is a versatile and effective method of making colloidal PnChI (Pn = Sb, Bi; Ch = S, Se) and $Sn_2PnS_2I_3$ (Pn = Sb, Bi) chalcohalides of tunable sizes and compositions. Furthermore, we demonstrate the preparation of mixed-pnictide chalcohalides through direct hot-injection and/or postsynthetic cation exchange, the latter being one of the few reported instances in chalcohalides. Additionally, we use the thiocyanate heat-up approach in combination with density functional theory to study halide mixing in quaternary tin chalcohalides. By pushing the limits of each synthetic technique, we have designed more soluble chalcohalides with tunable compositions while also gaining a better understanding of the efficacy of each procedure in respect to thin film and subsequent device fabrication. In addition to size and composition tuning, silyl hot-injection can help facilitate the future development and wide-scale application of chalcohalide-based devices by expanding the selection of solution-processable chalcohalides.

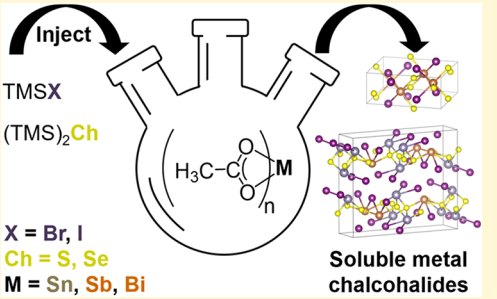

INTRODUCTION

Semiconductor nanocrystals play a growing role in modern day optoelectronics and energy conversion in areas such as light emitting displays (LEDs), biological imaging, photovoltaics, and photocatalysis.[1,2] Colloidal semiconductor nanocrystals in particular benefit from inherent solution processability, which allows for cheaper and often scalable deposition of inks by spin-casting, spray coating, and inkjet printing.[2−5] Thus, developing colloidal materials with ease of processing and device integration is essential in meeting the rising demands of the clean energy industry and to overcome the technological limitations presented by many current materials.[6] For example, colloidal lead halide perovskites are worldwide contenders in energy conversion due to their well-established defect tolerant optical properties and solution processability.[7] However, concerns about their stability and toxicity could restrict their widespread deployment. To overcome these challenges, it is reasonable to look at more stable, solution processable semiconductors with potentially improved biocompatibility and scalability.[1]

Chalcohalide semiconductors are quickly gaining traction as interesting alternatives to the more ubiquitous perovskites. These "split-anion" materials benefit from the inclusion of chalcogens which form stronger, more covalent bonds with the metal cation, increasing overall stability.[8−12] Similarly to perovskites, the optical properties of chalcohalides are tunable through cation, chalcogen, and/or halogen substitution, allowing for a diverse set of possible applications in optoelectronics.[8,9,12−14] The colloidal synthetic chemistry of chalcohalides, however, is less developed compared to perovskites, necessitating further study.

Previous methods used to prepare low dimensional chalcohalides involve the reaction of metal thiocyanates with binary metal halides and chalcogenides in high boiling point coordinating solvents such as oleylamine and oleic acid.[15] Our group recently demonstrated the versatility of this thiocyanate heat-up approach to make ternary mixed halide $Pb_3SBr_xI_{4-x}$

Received: October 30, 2025
Revised: February 16, 2026
Accepted: February 20, 2026
Published: March 5, 2026

and quaternary $Pb_2PnS_2I_3$ (Pn = Sb or Bi) nanocrystals.[16,17] Notably, these chalcohalides show superior stability against air and moisture in comparison to lead halide perovskites which readily decompose under comparable conditions.[16,17] These observations inspired us to employ this synthetic approach to construct quaternary tin-based analogs ($Sn_2SbS_2I_3$ and $Sn_2BiS_2I_3$), which are predicted to be promising materials for photovoltaics.[18] Similar to the lead chalcohalides, we found that the tin chalcohalides are remarkably stable against moisture, oxygen, and heat. However, the particle sizes of the tin chalcohalides were much larger (700−1500 nm) than those of the lead chalcohalides (46−427 nm). These results underscore the advantages and limitations of different synthetic approaches in accessing chalcohalides of desired compositions and sizes. Their stark differences encouraged us to seek alternative procedures that may give access to smaller tin chalcohalide particles.

Recent studies show that some chalcohalide systems can be synthesized by using the reactive, organo-halide, and -chalcogenide precursors first popularized in the synthesis of nanocrystalline perovskites and earlier compositions.[19−22] Monodisperse ternary BiChX (Ch = S, Se; X = I, Br, Cl) nanocrystals, for example, can be synthesized by injecting trimethylsilyl chalcogenides, trimethylsilyl halides, and/or benzoyl halides into a solution containing metal carboxylates.[23] Furthermore, particle morphology can be tuned by changing the reactivity of the organohalide and organochalcogenide precursors.[23] The use of reactive organoelement precursors—usually delivered via hot-injection—to control composition, phase, and morphology is an attractive method of synthesizing chalcohalide semiconductors.

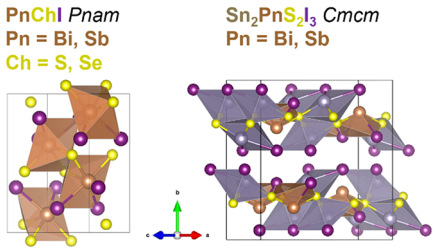

Figure 1. Crystalline unit cells of ternary PnChI *Pnam* and quaternary $Sn_2PnS_2I_3$ *Cmcm* chalcohalides (Ch = S, Se; Pn = Sb, Bi).

Here, we examine the hot-injection of silyl-halide and -chalcogenide precursors as a tool for accessing colloidal ternary SbChI and quaternary $Sn_2PnCh_2I_3$ (Ch = S, Se; Pn = Sb, Bi) nanocrystals (Figure 1). This proves to be a reliable method for making complex chalcohalides with opportunities for size and composition control. Furthermore, the use of multiple precursors or postsynthetic cation exchange enables pnictide mixing and consequent control over optical properties. Preliminary thin film fabrication through thermal evaporation of bulk chalcohalides underscores the importance of making smaller nanocrystals better suited for solution processing. Lastly, we use computational methods to better understand chalcohalide compositions and their different polymorphs.

METHODS

Materials

All commercially available chemicals were used as received. Antimony(III) acetate ($Sb(OAc)_3$, 97%), tin(II) acetate ($Sn(OAc)_2$, 99%), and tin(II) sulfate ($SnSO_4$, 95%) were purchased from Strem; iodotrimethylsilane (TMSI, 97%), bis-trimethylsilyl sulfide ($(TMS)_2S$, 98%), bismuth(III) acetate ($Bi(OAc)_3$, 99.99%), sodium thiocyanate (NaSCN, 98%), 1-octadecene (ODE, technical grade, 90%), and oleic acid (technical grade, 90%) from Sigma-Aldrich; antimony(III) bromide ($SbBr_3$, 99%), antimony(III) selenide (Sb_2Se_3, 99.999%), hexanes (99.9%), and methanol (99.9%) from Thermo-Fischer; bis-trimethylsilyl selenide ($(TMS)_2Se$) from Gelest.

Hot Injection Synthesis of Ternary and Related Chalcohalides

Unless noted otherwise, all syntheses were performed under air-free conditions (N_2 or Ar atmosphere) using standard Schlenk techniques. *SbSI*. The synthesis of SbSI was adapted from the previously reported synthesis of BiSI.[23] $Sb(OAc)_3$ (0.3 mmol, 89 mg), ODE (3 mmol, 0.79 g), and oleic acid (12.6 mmol, 3.56 g) were added to a 100 mL three-necked round-bottom flask equipped with a stir bar and thermocouple. The reaction flask was degassed under vacuum at 80 °C for 1 h. The mixture was heated to 110 °C until a clear, colorless solution formed. After cooling to 80 °C and degassing for three more cycles,[23] the flask was heated to 110 °C. Separately, in a N_2-filled glovebox, $(TMS)_2S$ (0.3 mmol, 54 mg), TMSI (0.3 mmol, 60 mg), and degassed ODE (6 mmol, 1.58 g) were added to a vial. The vial was capped with a septum, removed from the glovebox, and the solution was carefully injected into the reaction flask via syringe. After 1 min, the heating mantle was removed, and the flask immediately placed in an ice bath to cool. The solution was centrifuged at 4500 rpm for 5 min. The supernatant was discarded, and the solids were resuspended in hexanes (5 mL) and reprecipitated with methanol (5 mL), sonicating after each addition. This process was repeated until the supernatant was clear and colorless (>3 times). Solid SbSI and similar chalcohalides were stored under air at ambient conditions. *BiSI*. Prepared in a similar manner to SbSI by replacing $Sb(OAc)_3$ with $Bi(OAc)_3$ (0.3 mmol, 120 mg), using an injection temperature of 180 °C and a reaction time of 10 min. *SbSeI*. Prepared in a similar manner to SbSI by replacing $(TMS)_2S$ with $(TMS)_2Se$ (0.3 mmol, 68 mg) under identical reaction conditions. *$Sb_{1-x}Bi_xSI$ (direct)*. Prepared in a similar manner to SbSI using a mixture of $Sb(OAc)_3$ (0.15 mmol, 45 mg) and $Bi(OAc)_3$ (0.15 mmol, 60 mg) in ODE (12 mmol, 3.156 g) and oleic acid (3.15 mmol, 0.89 g) with an injection temperature of 150 °C. After 15 min at 150 °C, the flask was further heated to 180 °C. After 45 min, the heating mantle was removed and allowed to cool to room temperature. *$Sb_{1-x}Bi_xSI$ (cation-exchange)*. SbSI was prepared as described above with slight modifications to the amounts of ODE (12 mmol, 3.156 g), oleic acid (3.15 mmol, 0.89 g), and injection temperature (150 °C). Separately and simultaneously, a solution containing $Bi(OAc)_3$ (0.15 mmol, 60 mg) in ODE (12 mmol, 3.156 g) and oleic acid (3.15 mmol, 0.89 g) was prepared in a similar manner as in the synthesis of BiSI. The bismuth carboxylate solution was heated to 150 °C and injected into the crude solution of SbSI. After 15 min, the heating mantle was removed, and the reaction flask was immersed in an ice bath to cool rapidly. *$Sn_2SbS_2I_3$*. $Sn(OAc)_2$ (0.3 mmol, 71 mg), diphenyl ether (16 g, 94 mmol), and oleic acid (12.6 mmol, 3.56 g) were added to a three-neck round-bottom flask equipped with a stir bar and thermocouple. $Sb(OAc)_3$ (0.15 mmol, 45 mg), oleic acid (1.5 mmol, 430 mg), and ODE (5.7 mmol, 1.5 g) were added to a separate three-neck round-bottom flask equipped with a stir bar and thermocouple. Both reaction flasks were degassed under vacuum at 80 °C for 1 h. Each flask was then heated under Ar at 110 °C for 1 h. Then, each solution was cooled to 80 °C and degassed for 3 cycles. The tin carboxylate solution was then injected into the antimony carboxylate solution, and the combined solution was heated to 110 °C. Separately, in an N_2-filled glovebox, $(TMS)_2S$ (0.3 mmol, 54 mg), TMSI (0.5 mmol, 100 mg), and degassed ODE (6 mmol, 1.58 g) were added to a vial. The vial was

https://doi.org/10.1021/acs.chemmater.5c02918
Chem. Mater. 2026, 38, 2755−2766

capped with a septum, removed from the glovebox, and the solution was carefully injected into the reaction flask via syringe. The solution was then heated to 255 °C. After 1 min at 255 °C, the heating mantle was removed, allowing the flask to cool to room temperature. The resulting solids were isolated and purified via centrifugation in a similar manner as SbSI, discussed above. *$Sn_2BiS_2I_3$*. Prepared in a similar manner to $Sn_2SbS_2I_3$ using $Bi(OAc)_3$ (0.15 mmol, 60 mg), increasing the amount of TMSI (0.65 mmol, 130 mg), and using a reaction temperature of 225 °C. *$Sn_2Sb_{1-x}Bi_xS_2I_3$*. Prepared in a similar manner to $Sn_2SbS_2I_3$ using a mixture of $Bi(OAc)_3$ (0.15 mmol, 60 mg) and $Sb(OAc)_3$ (0.15 mmol, 45 mg) and a reaction temperature of 130−225 °C.

Heat-up Synthesis of Quaternary Chalcohalides

Quaternary bismuth and antimony mixed-halide chalcohalides were prepared via a previously reported heat-up procedure with slight modifications.[18,24] *$Sn(SCN)_2$*. The $Sn(SCN)_2$ precursor was prepared according to a previously reported procedure with slight modifications.[24] $SnSO_4$ (19 mmol, 4 g) and 1.0 M H_2SO_4 (4 mL) were added to deionized water (21 mL). This solution was slowly added to a solution containing NaSCN (74 mmol, 6 g) in deionized water (25 mL). After standing 5 h at room temperature and overnight in a fridge at 7 °C, the precipitated $Sn(SCN)_2$ was filtered and washed with deionized water. The white crystals were dried under vacuum and stored under air in ambient conditions. *$Sn_2SbS_2I_{3-x}Br_x$*. $Sn(SCN)_2$ (94 mg, 0.4 mmol), SbI_3 (0−0.2 mmol, 0−100 mg,) and/or $SbBr_3$ (0−0.2 mmol, 0−72 mg), ODE (24 mmol, 6.32 g) and oleic acid (6.30 mmol, 1.78 g) were added to a 100 mL three-necked round-bottom flask and heated to 300 °C for 30 s in air under ambient conditions. Solids were isolated by centrifugation at 4500 rpm for 5 min. The supernatant was discarded, and the solids resuspended in hexanes (5 mL) and reprecipitated with methanol (5 mL), sonicating after each addition. This process was repeated until the supernatant was clear and colorless (>3 times). *$Sn_2BiS_2I_{3-x}Br_x$*. Prepared and purified under identical conditions to $Sn_2SbS_2I_{3-x}Br_x$ using $(Sn(SCN)_2$ (94 mg, 0.4 mmol)), BiI_3 (0−0.2 mmol, 0−118 mg,) and/or $BiBr_3$ (0−0.2 mmol, 0−72 mg), SnI_2 (0−0.2 mmol, 0−75 mg) and/or $SnBr_2$ (0−0.2 mmol, 0−56 mg).

Scale up of Quaternary Chalcohalides. $Sn_2SbS_2I_3$ (2.5×)

$Sn(SCN)_2$ (1.0 mmol, 235 mg), SbI_3 (0.5 mmol, 250 mg), ODE (60 mmol, 15.8 g) and oleic acid (15.8 mmol, 4.4 g) were added to a 250 mL three-necked round-bottom flask and heated to 300 °C for 15 min in air. Solids were isolated by centrifugation at 4500 rpm for 5 min. The supernatant was discarded, and the solids resuspended in hexanes (5 mL) and reprecipitated with methanol (5 mL), sonicating after each addition. This process was repeated until the supernatant was clear and colorless (>3 times). Resulting yields were between 0.18 and 0.25 g. *$Sn_2BiS_2I_3$* (5×). Prepared and purified under identical conditions to $Sn_2SbS_2I_3$ using $Sn(SCN)_2$ (2.0 mmol, 470 mg), BiI_3 (1.0 mmol, 590 mg,), SnI_2 (1.0 mmol, 375 mg). Resulting yields were between 0.90 and 1.00 g.

Thermal Evaporation

$Sn_2SbS_2I_3$ (250 mg, 0.31 mmol) or $Sn_2BiS_2I_3$ (250 mg, 0.28 mmol) was placed in an evaporator crucible, the pressure was reduced to less than 10^{-5} Torr, and each sample heated from room temperature up to the point at which evaporation was detected by a Quartz Crystal Microbalance (QCM) similar to previous work.[25] *Thin film characterization*. The thin films were deposited onto a fluorine doped tin oxide (FTO) substrate and were analyzed by energy dispersive X-ray spectroscopy (EDS) and powder XRD. A simple device stack composed of FTO, TiO_2 compact layer (about 30 nm, as the electron transport layer), the evaporated chalcohalide thin film (as the absorber), 2,2′,7,7′-Tetrakis[*N*,*N*-di(4-methoxyphenyl)amino]-9,9′-spirobifluorene (200 nm, as the hole transport layer), and a gold layer (70 nm).[26] Current−voltage measurements were carried out on the devices.

Caution

$(TMS)_2S$ readily hydrolyzes to toxic H_2S gas in the presence of air, releasing a pungent odor. Anything exposed to $(TMS)_2S$ (i.e., glassware, syringes, etc.) should be cleaned with dilute bleach to quench residual odor prior to its proper disposal. TMSI and $(TMS)_2Se$ react violently with water and hydrolyze in the presence of air. These chemicals should only be handled under strictly air-free conditions.

Structural Characterization

Powder X-ray diffraction (XRD) patterns were collected using a zero-background quartz sample holder in a Rigaku Ultima IV diffractometer (40 kV, 44 mA) with Cu Kα radiation (λ = 1.54 Å). All Scherrer sizes and relative phase purities (weight percents) were determined using Match! phase identification software.[27] A JEOL JSM-IT200 scanning electron microscope (SEM) equipped with an X-ray detector was used to acquire SEM images and obtain relative elemental compositions of each sample. Transmission electron microscopy (TEM) images were collected on a JEOL 2100 scanning TEM. Each TEM sample was prepared by drop casting a dilute solution of chalcohalides suspended in toluene onto a carbon coated 200-mesh copper grid.

Optical Characterization

Diffuse reflectance spectra were measured with an SL1 Tungsten Halogen lamp (vis-IR), SL3 Deuterium Lamp (UV), and BLACK-Comet C-SR-100 spectrometer (200−1080 nm). Band gaps were estimated using the reported Tauc method which involves extrapolating the slope of $(Ah)^r$ graphed against $h\nu$.[28] A is defined as the absorbance, $h\nu$ is defined as the incident photon energy in eV, and r equals 1/2 (indirect band gap semiconductors) or 2 (direct band gap semiconductors).

Solid-State ^{77}Se NMR spectroscopy

All the SSNMR experiments were performed with a Bruker 4.0 mm HX MAS probe configured in ^{1}H−^{77}Se mode on a Bruker wide-bore 9.4 T [$\nu_0(^1H)$ = 400 MHz] NMR spectrometer equipped with a Bruker Advance III HD console. ^{77}Se SSNMR spectrum of Sb_2Se_3 was acquired with a 50 s delay, 2 CPMG loops, 840 scans, 41.6 kHz RF power at 10 kHz MAS frequency. The ^{77}Se SSNMR spectrum of SbSeI was acquired with a 50 s delay, 25 CPMG loops, 1200 scans, 41.6 kHz RF power at 10 kHz MAS frequency. ^{1}H chemical shifts were referenced to tetramethylsilane using adamantane [$\delta_{iso}(^1H)$ = 1.82 ppm] as a secondary standard. ^{77}Se chemical shifts were referenced indirectly to the established chemical shift scale ([$SeMe_2$, $\delta_{iso}(^{77}Se)$ = 0 ppm]) using the previously published relative NMR frequencies.[29]

Electronic Structure Calculations

Electronic structure calculations were carried out using the Vienna Ab-initio Simulation Package (VASP)[30] and the Tight Binding Linear Muffin-tin Orbital Atomic Sphere Approximation (TB-LMTO-ASA) package.[31] The band structure and DOS were calculated using the tetrahedron method after converging the total energy on a k-mesh of $1/a \times 1/b \times 1/c$ in the irreducible wedge of the Brillouin zone. All the unit cell representations were generated using VESTA.[32]

RESULTS AND DISCUSSION

Multinary Chalcohalides from Silyl Precursors

Recent phase evolution studies demonstrated that heating thiocyanate and iodide precursors of tin, antimony, and bismuth in a mixture of oleic acid and 1-octadecene (ODE) under air forms ternary chalcohalides starting at about 225−250 °C.[18] Higher order quaternary chalcohalides $Sn_2SbS_2I_3$ and $Sn_2BiS_2I_3$ become phase pure at 300 °C. Unfortunately, heterogeneous nucleation, coalescence, and particle aggregation are more favorable than homogeneous nucleation at this temperature, resulting in relatively large, insoluble ca. 700−1500 nm particles. To solve the limitation of this heat-up

https://doi.org/10.1021/acs.chemmater.5c02918
Chem. Mater. 2026, 38, 2755−2766

approach, we sought to find more reactive precursors that could give access to smaller, more soluble chalcohalide nanocrystals through more rapid, homogeneous nucleation.

Recent reports on $AgBiSCl_2$ and other bismuth-containing chalcohalide nanocrystals inspired us to examine hot-injection of silyl precursors as an alternative method.[23,33,34] In this reaction, the oxophilic silyl groups in trimethylsilyl (TMS)-based precursors such as $(TMS)_2Ch$ (Ch = sulfide or selenide) and TMSI (iodide) react with acetates and/or oleates in solution, while at the same time delivering chalcogen and halogen to the medium.[20,21,36,37] Outside of the initial reports, the preparation of antimony and tin-based chalcohalides through hot-injection of silyl precursors has received limited attention, opening an opportunity to examine these systems under a different synthetic lens.

Here, we first focused on ternary systems to gain a better understanding of the effect of pnictogen composition on their synthesis. The hot-injection of $(TMS)_2S$ and TMSI precursors into a solution of antimony or bismuth acetate in oleic acid and ODE at temperatures ranging from 110−160 °C under a dry (N_2 or Ar) atmosphere results in the near instantaneous formation of red SbSI or black BiSI[23] (Scheme 1a). Powder X-ray diffraction (XRD) of solids isolated from aliquots taken between 1−15 min after injection confirms that phase pure SbSI forms in as little as 1 min, while BiSI requires over 10 min to become phase pure (Figure 2 and Table 1). This method also succeeds in the preparation of SbSeI, specifically by replacing $(TMS)_2S$ with an equimolar amount of $(TMS)_2Se$ and injecting it alongside TMSI into a solution of antimony carboxylates in oleic acid and ODE at 110 °C. After 1 min reaction, powder XRD shows phase-pure SbSeI (Figure 2). Short reaction times (1 min) maximize phase purity while much longer reaction times (>15 min) result in Sb_2Se_3 impurities.

Scheme 1. Synthesis of Multinary Chalcohalides and Their Alloys by Hot-Injection and Post-Synthetic Cation Exchange

Hot-injection

(a) $Pn(OAc)_3$ —[$(TMS)_2Ch$, (TMS)I; ODE, oleic acid, Ar]→ $Sb_{1-x}Bi_xChI$
Pn = Sb and/or Bi; Ch = S or Se; T = 110–180 °C; t = 1–60 min

(b) $Pn(OAc)_3$ —[(1) $Sn(OAc)_2$; (2) $(TMS)_2S$, (TMS)I; ODE, Ph_2O, oleic acid, Ar]→ $Sn_2Sb_{1-x}Bi_xS_2I_3$
Pn = Sb and/or Bi; T = 110–250 °C; t = 1–60 min

Cation exchange

(c) SbSI —[$Bi(OAc)_3$; ODE, oleic acid, Ar]→ $Sb_{1-x}Bi_xSI$
T = 150 °C; t = 1–15 min

To further assess the structure and purity of some of the ternary chalcohalides, we measured the ^{77}Se solid-state nuclear magnetic resonance spectrum (SSNMR) of SbSeI as well as of commercially acquired, bulk (polycrystalline) Sb_2Se_3 as a hypothetical impurity. Interestingly, both samples display close—though not equal—isotropic chemical shifts at 158 and 145 ppm, respectively—see Supporting Information (SI) file. This is likely due to the similar coordination environments around the selenium sites in both structures. More specifically, each selenium atom is coordinated with 3 antimony atoms in a pyramidal-like fashion. While the structural similarities help explain the small difference in chemical shifts, powder XRD unambiguously shows that the phase pure SbSeI lacks any crystalline binary Sb_2Se_3 impurity.

Multiple Means of Size Control and One-Dimensional Assembly

Because Si−O bonds are much stronger than Si−Ch and Si−I bonds, the silyl precursors used here are very prone to react.[35] More specifically, TMS halides and chalcogenides are known to readily react with acetates and carboxylates.[20,21,36,37] This can help boost nuclei production, leading to smaller particles. The specific temperature and time used in the reaction significantly affect particle size (Figure 3). For example, when the synthesis of SbSI is run for 1 min, lowering the (injection and growth) temperature from 160 to 110 °C decreases the single crystalline (Scherrer) size from over 100 nm to ca. 40 nm, respectively. Furthermore, when the same reaction is run at 110 °C, shortening the reaction time from 15 to 1 min decreases the Scherrer size from over ca. 90 nm to ca. 40 nm. Surfactant (oleic acid) concentration also plays a role in determining Scherrer size. For example, increasing surfactant concentration from 0.5 to 1.8 M at 110 °C for 1 min decreases the Scherrer size of SbSI by ∼30%, from ca. 40 to 30 nm.

Scanning electron microscopy (SEM) images show that SbSI and SbSeI prepared by hot-injection adopt a long rod morphology with diameters between 100−500 nm and lengths of up to 5−10 mm (Figure 4 and SI). Ternary chalcohalides exhibit preferred growth along the *c* (*z*) direction of the *Pnam* unit cell, perpendicular to the (002) set of lattice planes.[23,34,35] However, upon close examination of the powder XRD patterns of SbSI and SbSeI, the telltale signs of this pronounced 1D anisotropy would appear to be missing. For example, all the individual reflections in the powder XRD of SbSI are similarly broadened, with Scherrer sizes ranging relatively little between 41 ± 17 nm. The (002) reflection, which could be expected to be very narrow because it stems from the planes which stack along the direction of growth of the nanorods is just as wide as the rest of all reflections, with a Scherrer size of only ∼30 nm. In all, analysis of over 20 unique reflections across the powder XRD pattern of SbSI reveals that the largest dimension fails to exceed 80 nm. The same is true for SbSeI (Table S1).

To better understand the apparent discrepancy between the large aspect ratio observed under the SEM and the lack of anisotropy present in the powder XRD, we resorted to higher resolution, transmission electron microscopy (TEM). Using SbSeI as an example, TEM shows that each chalcohalide nanorod is indeed polycrystalline, containing a collection of ellipsoidal domains along its whole length. The sizes of these domains range from ca. 20−50 nm, which closely matches the average calculated Scherrer sizes of 30 ± 20 nm. In other words, TEM shows that the rods are discontinuous or effectively (multi)twinned, containing a collection of smaller crystallites which assemble into the long, bundled rods observed by SEM. Interestingly, similar behavior was reported for BiSI nanorods synthesized in water.[38]

Band Gap Tuning via Pnictide Mixing

Tauc plots[26] made from diffuse reflectance measurements show that SbSI, SbSeI, and BiSI prepared by hot-injection have approximate band gaps of 1.95, 1.50, and 1.55 eV, respectively

https://doi.org/10.1021/acs.chemmater.5c02918
Chem. Mater. 2026, 38, 2755−2766

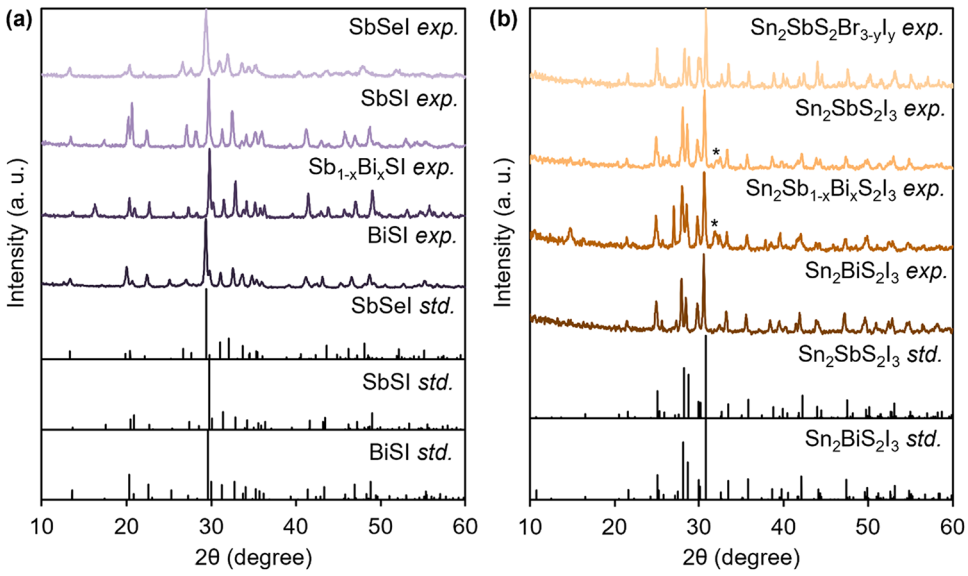

Figure 2. Powder XRD patterns of (a) PnChI (Pn = Bi, Sb; Ch = S, Se; x = 0.2) and (b) $Sn_2PnS_2X_3$ (Pn = Sb, Bi; x = 0.2; X = I, Br; y = 0.6). Conditions: [Sn] = 13−40 mM, [Pn] = 20−43 mM, [Ch] = 13−80 mM, [X] = 13−60 mM, [Oleic acid] = 0.5−1.8 M. (* = Minor SnS fraction).

(Figure 5), which agrees well with literature data.[39−43] Estimated Bohr radii for SbSI, SbSeI, and BiSI range from 5−10 nm, suggesting that the particles, while soluble, remain too large to exhibit quantum confinement (Table S2).[44] These ternary chalcohalides display weak PL emission. (Figure S9). SbSeI has been reported to be luminescent,[36] however our SbSeI lacks measurable PL in the ultraviolet (UV), visible (Vis), or infrared (IR) regions of the spectrum.

Elemental alloying can be a powerful tool to fine-tune the optical activity of semiconductor nanocrystals across the electromagnetic spectrum.[17,45−47] For instance, solar cells based on $Sb_{0.67}Bi_{0.33}SI$ chalcohalide thin films with an intermediate band gap of 1.62 eV, prepared via chemical bath deposition on TiO_2, achieved an impressive PCE of 4.07%.[48] The lattice mismatch between *Pnam* structures of SbSI and BiSI is under 3%, while the difference in ionic sizes in going from Sb(III) to Bi(III) is as small as 2% (Table S3). The small lattice mismatch between ternary chalcohalides and relative ionic radii between Pn(III) sites prompted us to investigate whether alloyed mixed-pnictide chalcohalide nanocrystals with compositionally tunable optical properties could be attainable through colloidal synthesis.

Injecting $(TMS)_2S$ and TMSI into an equimolar mixture of bismuth and antimony carboxylates in ODE and oleic acid at 150 °C quickly (<1 min) results in the formation of a black solution closely resembling BiSI. Powder XRD matches the standard patterns of *Pnam* SbSI and BiSI, without detectable crystalline impurities (Figure 2). The similarities between these two patterns make it difficult to identify the composition or elemental distribution of the mixed-pnictide chalcohalides from regular powder XRD alone. For instance, the most intense reflection, $(1\bar{1}2)$, occurs between 29.50−29.90° 2θ. To overcome this limitation, we resorted to optical spectroscopy and SEM, including elemental analysis by energy dispersive X-ray spectroscopy (EDS).

EDS analysis of nanocrystalline solids isolated from the hot-injection reaction after 1 min, 15 min, and 1 h at 150−180 °C show compositions of $Sb_{0.7}Bi_{0.3}S_{0.9}I_{0.9}$, $Sb_{0.8}Bi_{0.2}S_{0.8}I_{1.0}$, and $Sb_{0.5}Bi_{0.5}S_{0.9}I_{1.2}$, respectively (Table 1). However, the Tauc band gaps derived from diffuse reflectance data for all these samples remain in the 1.55−1.59 eV range, which is very close to that of pure BiSI (Figure 6b). This indicates that $Sb_{1-x}Bi_xSI$ nanocrystals prepared in this manner exhibit significant band gap bowing. Previous observations of non-Vegard behavior in $Sb_{1-x}Bi_xSI$ support this idea.[49,50] Because optical tunability is useful in different device applications, we explored alternative methods to achieve pnictide mixing.

Postsynthetic Cation Exchange and Evolution of $Sb_{1-x}Bi_xSI$ Morphology

While heavily utilized in chalcogenide chemistry,[51−53] cation exchange remains underutilized in the case of chalcohalides. We find that injecting a solution of bismuth carboxylate into a solution of freshly prepared SbSI at 150 °C produces an immediate color change from the initial deep orange to black, resembling the color of BiSI (see Methods section). EDS analysis of nanocrystalline solids isolated from this cation exchange reaction after 1 and 15 min show antimony-rich compositions of $Sb_{0.8}Bi_{0.2}S_{1.0}I_{0.9}$ and $Sb_{0.8}Bi_{0.2}S_{1.0}I_{1.1}$, respectively (Table 1). Tauc band gaps derived from diffuse reflectance data reveal band gaps of 1.60 and 1.70 eV, respectively (Figure 6b). In contrast to the non-Vegard behavior of $Sb_{1-x}Bi_xSI$ nanocrystals prepared directly by hot-injection, these results indicate that postsynthetic cation exchange enables both pnictide mixing and subsequent control over optical properties. Notably, TEM images demonstrate that mixed pnictide chalcohalides prepared by either direct hot-injection or postsynthetic cation exchange exist as discrete nanocrystals (Figure 7), as opposed to the parent compositions such as SbSI and SbSeI, which aggregate into one-dimensional assemblies (Figure 4c). This suggests that pnictide mixing suppresses particle aggregation and assembly.

Electron micrographs reveal that the morphology of the $Sb_{1-x}Bi_xSI$ nanocrystals evolves depending on their method of synthesis (Figure 7). In the case of direct hot-injection, we observe near spheroidal, 72 nm × 91 nm $Sb_{1-x}Bi_xSI$ nanocrystals with a slightly prolate aspect ratio of 1.3 after 1 min. These begin to elongate to 56 nm × 179 nm nanorods with an aspect ratio of 3.2 after 15 min. They further elongate to 126 nm × 469 nm nanorods with an aspect ratio of 3.8 after

https://doi.org/10.1021/acs.chemmater.5c02918
Chem. Mater. 2026, 38, 2755−2766

Table 1. Synthetic Conditions and Resulting Properties of Solution-grown Ternary and Quaternary Chalcohalides[a]

prec./mmol	solvent(s)/mL	inj./mmol	$T_{inj.}$/°C	T_{growth}/°C	t/min	single crystalline domain[b] (SEM)/nm	product(s)[c] (band gap/eV)[d]
		Ternary Chalcohalides					
$Sb(OAc)_3$ (0.3)	ODE (3) + oleic acid (4)	$(TMS)_2S$ (0.3) + TMSI (0.3)	110	110	1	32 ± 19	SbSI (1.95)
$Sb(OAc)_3$ (0.3)	ODE (6) + oleic acid (1)	$(TMS)_2S$ (0.3) + TMSI (0.3)	110	110	1	41 ± 17	$SbS_{0.8}I_{1.0}$ (1.95)
$Sb(OAc)_3$ (0.3)	ODE (3) oleic acid (4)	$(TMS)_2Se$ (0.3) + TMSI (0.3)	110	110	1	30 ± 20	SbSeI (1.50)
$Sb(OAc)_3$ (0.3)	ODE (6) + oleic acid (1)	$(TMS)_2S$ (0.3) + TMSI (0.3)	150	150	1	34 ± 13 (6100 × 420)	SbSI (1.95)
SbSI (0.3)	ODE (10) + oleic acid (2)	$Bi(OAc)_3$ (0.15)	150	150	1	52 ± 31 (1200 × 190)	$Sb_{0.8}Bi_{0.2}S_{1.0}I_{0.9}$ (1.60)
SbSI (0.3)	ODE (10) + oleic acid (2)	$Bi(OAc)_3$ (0.15)	150	150	15	94 ± 89 (2000 × 350)	$Sb_{0.8}Bi_{0.2}S_{0.8}I_{1.1}$[b] (1.70)
$Sb(OAc)_3$ (0.15) + $Bi(OAc)_3$ (0.15)	ODE (6) + oleic acid (1)	$(TMS)_2S$ (0.3) + TMSI (0.3)	150	150	1	80 ± 59 (91 × 72)	$Sb_{0.7}Bi_{0.3}S_{0.9}I_{0.9}$ (1.55)
$Sb(OAc)_3$ (0.15) + $Bi(OAc)_3$ (0.15)	ODE (6) + oleic acid (1)	$(TMS)_2S$ (0.3) + TMSI (0.3)	150	150	15	65 ± 18 (198 × 98)	$Sb_{0.8}Bi_{0.2}S_{0.8}I_{1.0}$[b] (1.59)
$Sb(OAc)_3$ (0.15) + $Bi(OAc)_3$ (0.15)	ODE (6) + oleic acid (1)	$(TMS)_2S$ (0.3) + TMSI (0.3)	150	180	60	89 ± 86 (469 × 126)	$Sb_{0.5}Bi_{0.5}S_{0.9}I_{1.2}$ (1.59)
$Bi(OAc)_3$ (0.3)	ODE (6) oleic acid (1)	$(TMS)_2S$ (0.3) + TMSI (0.3)	160	160	10	36 ± 16	BiSI (1.55)
		Quaternary Chalcohalides					
$Bi(OAc)_3$ (0.15)	ODE (3.9) + oleic acid (4.48) + Ph_2O (15)	$Sn(OAc)_2$ (0.3), $(TMS)_2S$ (0.3) + TMSI (0.65)	80, 110	225	0	68 ± 23	$Sn_2BiS_2I_3$ (1.40)
$Sb(OAc)_3$ (0.15)	ODE (3) + oleic acid (4.15) + Ph_2O (15)	$Sn(OAc)_2$ (0.3), $(TMS)_2S$ (0.3) + TMSI (0.5)	80, 110	255	0	51 ± 11	$Sn_2SbS_2I_3$ (1.90)
$Sb(OAc)_3$ (0.15) + $Bi(OAc)_3$ (0.15)	ODE (3.9) + oleic acid (4.48) + Ph_2O (15)	$Sn(OAc)_2$ (0.3), $(TMS)_2S$ (0.3) + TMSI (0.5)	80, 110	190	0	39 ± 22	$Sn_{5.0}Sb_{0.8}Bi_{0.2}S_8I_{3.5}$[b] (1.80)
$Sb(OAc)_3$ (0.15) + $Bi(OAc)_3$ (0.15)	ODE (3.9) + oleic acid (4.48) + Ph_2O (15)	$Sn(OAc)_2$ (0.3), $(TMS)_2S$ (0.3) + TMSI (0.5)	80, 110	250	0	>200	$Sn_{1.8}Sb_{0.4}Bi_{0.6}S_{1.3}I_{2.7}$[b] (1.50)
		Halide Mixing					
$Sn(SCN)_2$ (0.4) + $SbBr_3$ (0.1) + SbI_3 (0.1)	ODE (8) + oleic acid (2)	N/A	N/A	300	1	>200	$Sn_{1.5}SbS_{1.6}I_{1.4}Br_{0.7}$[b]
$Sn(SCN)_2$ (0.4) + $SbBr_3$ (0.05) + SbI_3 (0.15)	ODE (8) + oleic acid (2)	N/A	N/A	300	1	>200	$Sn_{1.3}SbS_{1.6}I_{1.7}Br_{0.4}$
$Sn(SCN)_2$ (0.4) + $BiBr_3$ (0.2) + SnI_2 (0.2)	ODE (8) + oleic acid (2)	N/A	N/A	300	1	>200	94% $Sn_2BiS_2I_3$ + 6% $Bi_{13}Br_2S_{18}$

[a]ODE = 1-octadecene; TMS = trimethylsilyl. [b]Single crystalline domain or Scherrer sizes determined with Match! [c]Elemental compositions from EDS. [d]Determined from Tauc plots (see Methods section).

https://doi.org/10.1021/acs.chemmater.5c02918
Chem. Mater. 2026, 38, 2755−2766

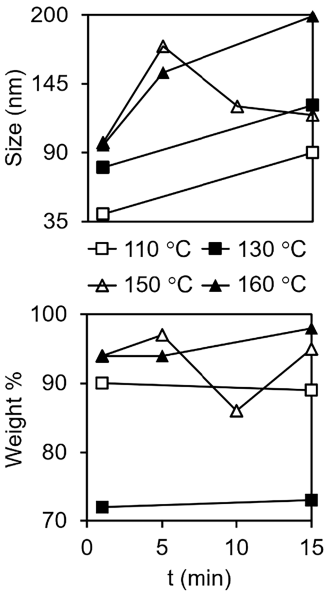

Figure 3. Effect of time and temperature on the size and phase purity of SbSI prepared by hot-injection ($[Sb^{3+}] = [S^{2-}] = [I^-] = 43$ mM, [oleic acid] = 0.5 M, see Methods section).

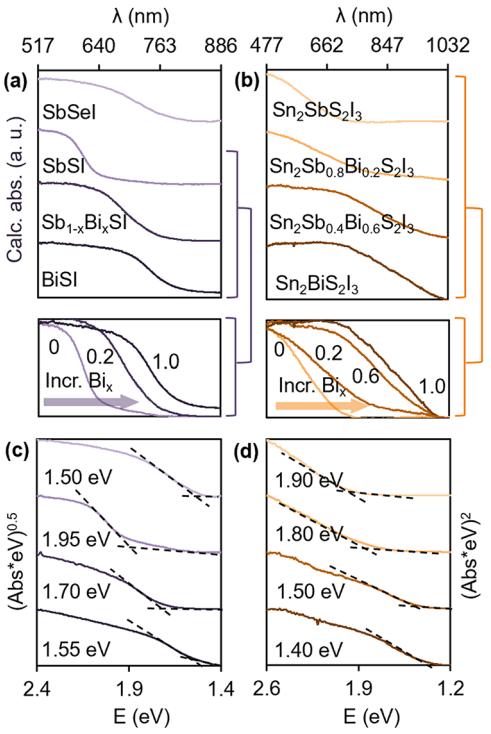

Figure 5. Diffuse reflectance spectra (a–b) and corresponding Tauc plots (c–d) of ternary (a, c; $x = 0.2$) and quaternary chalcohalides (b, d; $x = 0.2, 0.6$).

60 min. In the case of postsynthetic cation exchange, injection of bismuth carboxylate solution at 150 °C causes the disassembly of the aforementioned, 417 nm × 6.1 μm SbSI bundles into smaller ca. 60 nm crystallites. Further reaction results in 189 nm × 1.24 μm nanorods after 1 min, and 351 nm × 1.97 μm after 15 min—a decrease in aspect ratio from 6.6 to 5.6, respectively (Figure 7). Thus, while the diameters of all mixed pnictide chalcohalide nanorods remain in the 60–350 nm range, their lengths differ significantly depending on their method of preparation. Mixed pnictide chalcohalides prepared by hot-injection are shorter than 500 nm, while those prepared by cation exchange are longer than 1 μm. Direct synthesis by hot-injection of silyl precursors yields chalcohalides with smaller aspect ratios (1.3–3.8) compared to those prepared from postsynthetic cation exchange (5.6–6.6). Because aspect ratio is known to affect optical properties,[18] this suggests that morphology, rather than bismuth content, accounts for the aforementioned optical properties.

The classical topotactic cation exchange mechanism cannot account for the morphological changes observed by SEM, likely because pnictogen-chalcogen bonds are more covalent than transition metal-chalcogen bonds.[49] Instead, introduction of extra oleic acid during hot injection of $Bi(OAc)_3$ may initiate rapid dissolution of SbSI, followed by slower crystallization of smaller aspect ratio $Sb_{1-x}Bi_xSI$ nanorods. Further, a degree of lattice mismatch between SbSI and BiSI may result in partial exchange of Bi^{3+} with Sb^{3+} at the surface of the crystals, inducing strain and transiently creating hetero-

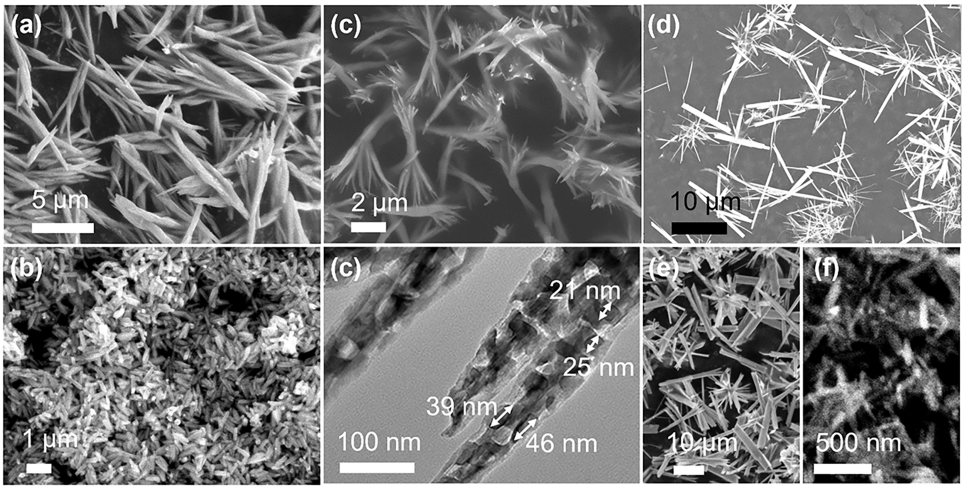

Figure 4. Representative SEM and TEM (SbSeI) images of (a) SbSI, (b) $Sb_{0.5}Bi_{0.5}S_{0.9}I_{1.2}$, (c) SbSeI, (d) $Sn_2BiS_2I_3$ (e), $Sn_{1.8}Sb_{0.4}Bi_{0.6}S_{1.3}I_{2.7}$, and (f) $Sn_2SbS_2I_3$ prepared by hot-injection.

https://doi.org/10.1021/acs.chemmater.5c02918
Chem. Mater. 2026, 38, 2755–2766

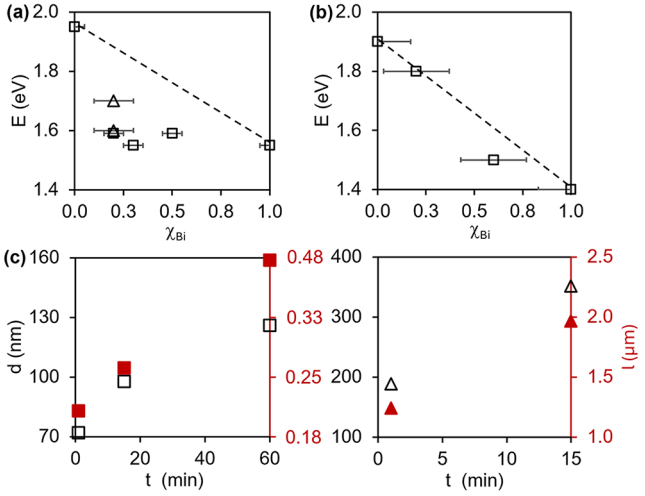

Figure 6. (a, b) Vegard plots showing the relationship between experimental band gap and composition ($\chi_{Bi} + \chi_{Sb} = 1$) for (a) $Sb_{1-x}Bi_xSI$ and (b) $Sn_2Sb_{1-x}Bi_xS_2I_3$ nanocrystals derived from direct hot-injection synthesis (□) or postsynthetic cation exchange (Δ). (c) Changes in the diameter (black) and length (red) of $Sb_{1-x}Bi_xSI$ nanocrystals made by direct hot-injection synthesis (□, red ■) or postsynthetic cation exchange (Δ, red ▲) over time.

structured crystals that more easily break apart during the earlier stages of reaction.[49,54]

Halide Mixing and Attempted Thin Film Fabrication from Quaternary Chalcohalides

While hot-injection of silyl precursors proves to be a valuable method toward accessing soluble chalcohalide semiconductors of various compositions, we were also drawn to exploring the possibilities and limits of the heat-up approach in terms of compositional tunability. Previous studies show that mixed halide $Pb_3SBr_xI_{4-x}$ chalcohalides with tunable emission can be made using this approach.[17] These results motivated us to explore lead-free, $Sn_2SbS_2I_{3-x}Br_x$. Powder XRD shows that systematic replacement of SbI_3 with equimolar amounts of $SbBr_3$ results in partial halide substitution along the $Sn_2SbS_2I_{3-x}Br_x$ series. Specifically, individual reflections shift to larger 2θ values as the bromine loading increases, indicating a contraction in the size of the *Cmcm* unit cell with the smaller halide (Figure S33). More specifically, as 0%, 25%, 50%, and 100% SbI_3 is replaced by $SbBr_3$, the $(11\bar{4})$ reflection of $Sn_2SbS_2I_3$ shifts from 30.76°, 30.82°, 30.90°, to 31.23° 2θ, respectively. Furthermore, EDS shows that as bromine loading increases from 25% to 50%, composition changes from $Sn_{1.3}SbS_{1.6}I_{1.7}Br_{0.4}$ to $Sn_{1.5}SbS_{1.6}I_{1.4}Br_{0.7}$. (Table 1). This approach has its limits, however, as full replacement of SbI_3 with $SbBr_3$ results in a mixture of binary sulfide impurities, as observed by powder XRD (Figure 2). Similarly, attempts to introduce Br into $Sn_2BiS_2I_{3-x}Br_x$ were unsuccessful and resulted in phase segregation into $Sn_2BiS_2I_3$ and $Bi_{6.33}BrS_9$ (Table 1). These results are unsurprising, as neither $Sn_2SbS_2Br_3$ nor $Sn_2BiS_2Br_3$ is reported in the ICSD structural database.

Motivated by the possibility of at least partial compositional and optoelectronic tuning, as well as photovoltaic[55] application of lead-free quaternary chalcohalide semiconductors, we scaled up by 5-fold the heat-up synthesis of $Sn_2SbS_2I_3$ and $Sn_2BiS_2I_3$ to 5 g each.[18] While this approach succeeds in generating multigram quantities of these materials without compromising phase purity, it yields relatively large (700−1500 nm), insoluble particles that make traditional methods of solution-phase processing (i.e., spin-casting) impractical. Just as ternary chalcohalide nanocrystals have been successfully spin coated to form functional optoelectronic devices, we were interested in fabricating thin films from these complex quaternary $Sn_2PnS_2X_3$ (Pn = Sb, Bi; X = Br, I) compositions. However, prior to reducing the particle size of these quaternary chalcohalides to enable solution processing, we first tested alternative means of thin film fabrication better suited for these existing bulk powders. Therefore, we attempted to prepare thin films of these materials via thermal evaporation (see Methods section). Unfortunately, residual black powder in the crucibles after evaporation suggests incomplete evaporation or decomposition of the chalcohalides. The XRD and EDS spectra (Figures S20−S22) of the evaporated thin films (50−100 nm) exhibit changes that suggest the presence of a mixture of binary halides and chalcogenides. Furthermore, current−voltage measurements of the devices containing thermally evaporated thin films does not exhibit rectifying behavior, as expected for these semiconductors. These findings suggest that further optimization is required to achieve proper deposition without degrading the chalcohalide phases found in the parent powders.

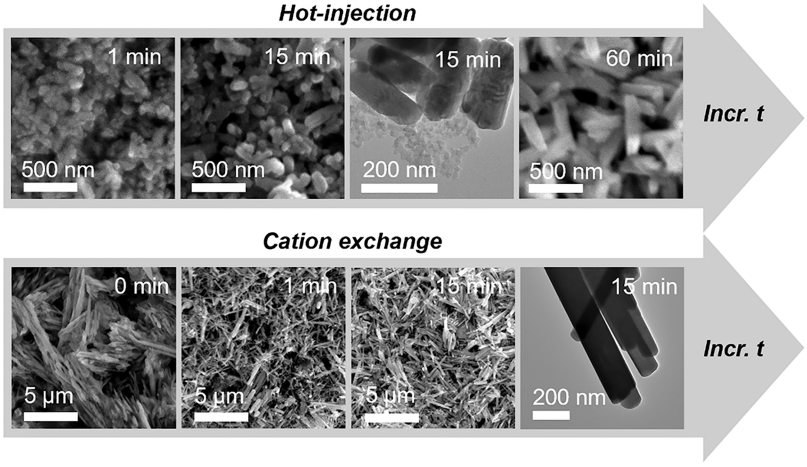

Figure 7. Representative SEM and TEM images of $Sb_{1-x}Bi_xSI$ nanocrystals prepared under different conditions.

https://doi.org/10.1021/acs.chemmater.5c02918
Chem. Mater. 2026, 38, 2755−2766

Soluble Quaternary Chalcohalides by Hot-injection

To synthesize smaller, $Sn_2SbS_2I_3$ and $Sn_2BiS_2I_3$ chalcohalides with increased solubility and processability, we resorted to hot-injection of silyl precurors. Injection of a mixture of $(TMS)_2S$ and TMSI into a freshly made solution of tin and bismuth or antimony carboxylates in oleic acid, ODE, and Ph_2O at higher temperatures (>190 °C) than those used to make ternary chalcohalides (<160 °C) produces 50−70 nm $Sn_2SbS_2I_3$ and $Sn_2BiS_2I_3$ nanocrystals. (Scheme 1b and Figure 2). The higher reactivity of TMS-based precursors as compared to metal halides and thiocyanates likely explains the decrease in particle size. Significantly, these quaternary tin chalcohalide nanocrystals are more soluble than their micron-size counterparts, suggesting they may be better suited for solution-phase processing. Like the ternary systems, Tauc plots show that the band gap of the quaternary, antimony- tin chalcohalides is wider (1.90 eV) than that of the bismuth-containing analogs (1.40 eV) (Figure 5). SEM images show that the nanocrystals occur as long nanorods with relatively homogeneous diameter and length distributions (Figure 4).

This hot-injection approach also enables the preparation of formally pentanary $Sn_2Sb_{1-x}Bi_xS_2I_3$ chalcohalides containing both antimony and bismuth (Figure 2). EDS shows that increasing the growth temperature from 190 to 250 °C raises the bismuth content from $Sn_{5.0}Sb_{0.8}Bi_{0.2}S_{8.0}I_{3.5}$ to $Sn_{2.5}Sb_{0.4}Bi_{0.6}S_{3.0}I_{2.3}$ (Table 1). (The slight tin- and sulfur-rich and iodine poor compositions suggest small amounts of tin sulfide impurities may be present.) Further, the same temperature change increases the Scherrer size of the crystallites from ca. 39 nm to >200 nm, while the band gaps narrow from 1.80 to 1.50 eV (Figure 6c). Therefore, unlike the band gap bowing observed in mixed ternary chalcohalides, quaternary chalcohalides display near ideal Vegard-like behavior (Figure 6b).

Polymorphism in Ternary and Quaternary Chalcohalides

To better understand the available phase space in complex chalcohalides, we used the Perdew−Burke-Ernzerhof (PBE) functional and the Vienna *ab initio* simulation package (VASP)[28] to compare the relative energies among different polymorphs. Very recently, the $Pna2_1$ polymorph of SbSI was reported to be the ground state at low (near the Curie) temperature.[49] In contrast, our calculations suggest that the *Pnam* polymorph may be slightly lower in energy. However, our calculations lack van der Waals (vdw) or spin−orbit coupling (SOC) corrections that can improve accuracy. More importantly, a comparison of the *Pnam*, $Pna2_1$, and $P2_12_12_1$ polymorphs of SbSI shows that a small, symmetry-lowering distortion in the arrangement of Sb and S atoms along the *c* axis transforms the centrosymmetric *Pnam* into the polar $Pna2_1$ structure.[56] Further, The $P2_12_12_1$ structure is higher in energy but is still very close in symmetry to that of *Pnam* and $Pna2_1$. Taken together, our results suggest that the *Pnam* and $Pna2_1$ polymorphs of SbSI may be very close in energy or nearly degenerate. Density of states (DOS) and band structure ab initio calculations of the three different SbSI phases underestimate the measured experimental optical gaps, as observed with other systems.[57,58] Specifically, VASP and LMTO calculations yield indirect band gaps of 1.5 eV (49% underestimate) and 0.9−1.0 eV (23%), respectively.

Because the ICSD lacks reported structures for the quaternary chalcohalide compositions $Sn_2SbS_2Br_3$, $Sn_2BiS_2Cl_3$, and $Sn_2BiS_2Br_3$, we created three polymorphs for each by selectively replacing pnictogen (Sb for Bi) and/or halide (I for Br) atoms in the reported *Cmcm* (mp-561134), $Cmc2_1$ (mp-1219046), and $P2_1/c$ (mp-578882) structures of $Pb_2SbS_2I_3$. An additional monoclinic polymorph ($P2/m$) results from coloring the mixed-cation sites in *Cmcm* (ICSD 47149) $Sn_2SbS_2I_3$.[48,59] The unreported $P2/m$ polymorph is a 64-atom superstructure formed by placing either Sn or Bi atoms in the mixed-cation positions in a −Sn−Sb-Sn−Sb−Sn−Sb− (ABABAB) configuration along the metal−sulfur chains. Interestingly, using the PBE functional, calculations predict this to be the lowest energy phase for all three compositions (Figure 8 and SI). Reduced repulsion between Sn-

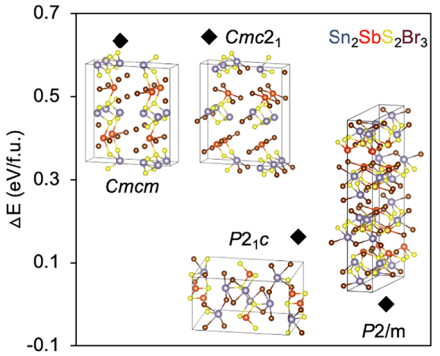

Figure 8. Relative energies between calculated polymorphs of quaternary $Sn_2SbS_2Br_3$ chalcohalides.

(polyhedra)−Sb(chain) can stabilize a particular structure through a reduction in Madelung energy and an increase in bonding between the Sn(polyhedra) and neighboring anions.[60,61] The theoretical $P2/m$ polymorph that we calculated contains such ordering (-ABABAB-), which helps stabilize its structure. However, only the relatively higher energy, *Cmcm* polymorph is observed here. As in the aforementioned ternary case, calculations suggest that a second metastable, $Cmc2_1$ polymorph may be isolable under the kinetically controlled conditions afforded by colloidal synthesis. Ongoing work in this direction will be reported in due course.

CONCLUSION

Both silyl hot-injection and thiocyanate heat-up approaches are suitable for synthesizing a multitude of chalcohalides from solution phase. These methods are extremely versatile in altering composition with respect to metal, chalcogen, and sometimes even the halogen. Furthermore, each procedure utilizes commercially available precursors and is performed under relatively mild reaction conditions. Nevertheless, we uncovered clear differences between the two procedures that may help guide future synthesis, property measurement, and device fabrication efforts. To target and control particle size, and to prepare smaller more soluble particles amenable to solution processing, silyl hot-injection is generally the preferred route. Based on prior literature evidence, we attribute this to the more reactive nature of the trimethylsilyl-based precursors as compared to simple binary halides. Additionally, pnictide mixing, either through direct hot-injection or postsynthetic cation exchange, offers control over optical properties in ternary and quaternary chalcohalide nanocrystals. On the other hand, optical tunability can also be achieved using the heat-up approach. Inspired by our previous work with halide mixing in

https://doi.org/10.1021/acs.chemmater.5c02918
Chem. Mater. 2026, 38, 2755−2766

ternary lead chalcohalides, we showed that partial halogen substitution may be possible in $Sn_2SbS_2I_{3-x}Br_x$. DFT suggests that the observed limitations and opportunities in the phase and composition-controlled synthesis and optical tuning of these materials may be due to the relative stability among different polymorphs ($Sn_2SbS_2X_3$). Overall, both synthetic methods provide valuable insight into the rational design of chalcohalides with desired particle size, composition, and optical properties.

We find that chalcohalides prepared by silyl hot-injection form relatively stable suspensions in toluene and are more suitable for solution phase processing compared to those prepared using the heat-up approach. Future experiments will be geared toward scaling up this hot-injection approach to form gram+ scale quantities of soluble multinary chalcohalides for thin film and subsequent device fabrication. We also plan to test these materials in photo- and electrocatalysis. Additionally, we are interested in studying cation-exchange in closer detail while also exploring chalcogen and halogen exchange in chalcohalides through similar techniques. Lastly, by utilizing TMS-based chalcogenides and halides along with widely available metal acetates, hot-injection may allow for the rapid synthetic development of other, less-explored metal chalcogenides and chalcohalides under similar conditions presented here, supporting the growing demand for stable and more biocompatible nanocrystalline semiconductors.

■ ASSOCIATED CONTENT

Supporting Information

The Supporting Information is available free of charge at https://pubs.acs.org/doi/10.1021/acs.chemmater.5c02918.

Additional SEM-EDS, TEM, diffuse reflectance, solid state NMR, powder XRD, TGA, thin film deposition schematic, JV scans, PL, and DFT calculations (PDF)

■ AUTHOR INFORMATION

Corresponding Author

Javier Vela − *Department of Chemistry, Iowa State University, Ames, Iowa 50011, United States; Ames National Laboratory, Ames, Iowa 50011, United States;* orcid.org/0000-0001-5124-6893; Email: vela@iastate.edu

Authors

Eve K. Stegner − *Department of Chemistry, Iowa State University, Ames, Iowa 50011, United States*

Md Riad Sarkar Pavel − *Department of Chemistry, Iowa State University, Ames, Iowa 50011, United States; Ames National Laboratory, Ames, Iowa 50011, United States*

Anuluxan Santhiran − *Department of Chemistry, Iowa State University, Ames, Iowa 50011, United States; Ames National Laboratory, Ames, Iowa 50011, United States*

Jack Lawton − *School of Materials Science and Engineering, Georgia Institute of Technology, Atlanta, Georgia 30332, United States*

Juan-Pablo Correa-Baena − *School of Materials Science and Engineering, Georgia Institute of Technology, Atlanta, Georgia 30332, United States;* orcid.org/0000-0002-3860-1149

Aaron J. Rossini − *Department of Chemistry, Iowa State University, Ames, Iowa 50011, United States; Ames National Laboratory, Ames, Iowa 50011, United States;* orcid.org/0000-0002-1679-9203

Complete contact information is available at: https://pubs.acs.org/10.1021/acs.chemmater.5c02918

Author Contributions

[‖]E.K.S. and M.R.S.P. contributed equally to this work. The manuscript was written through contributions of all authors. All authors have given approval to the final version of the manuscript.

Notes

The authors declare no competing financial interest.

■ ACKNOWLEDGMENTS

This work honors the outstanding contributions to the chemistry of materials by Mercouri Kanatzidis. This work was supported by the U.S. National Science Foundation, Division of Chemistry, Macromolecular, Supramolecular, and Nanochemistry Program (2305062) by a grant awarded to J.V. SSNMR work by A.S. and A.J.R. was supported by the U.S. Department of Energy (DOE) Ames National Laboratory, Materials Science and Engineering Division. Ames National Laboratory is operated for the U.S. DOE by Iowa State University, under contract no. DE-AC02-07CH11358. We thank Allie Roth and Gordie Miller for comments.

■ REFERENCES

(1) Buonsanti, R.; Cossairt, B. The Future of Colloidal Semiconductor Nanocrystals. *Chem. Mater.* **2025**, *37*, 1333−1334.

(2) Talapin, D. V.; Lee, J. S.; Kovalenko, M. V.; Shevchenko, E. V. Prospects of Colloidal Nanocrystals for Electronic and Optoelectronic Applications. *Chem. Rev.* **2010**, *110*, 389−458.

(3) de Arquer, F. P. G.; Amrin, A.; Meredith, P.; Sargent, E. H. Solution-Processed Semiconductors for Next-Generation Photodetectors. *Nat. Rev. Mater.* **2017**, *2*, No. 16100.

(4) Choi, J. H.; Wang, H.; Oh, S. J.; Paik, T.; Jo, P. S.; Sung, J.; Ye, J.; Zhao, T.; Diroll, B. T.; Murray, C. B.; Kagen, C. R. Exploiting the Colloidal Nanocrystal Library to Construct Electronic Devices. *Science* **2016**, *352*, 205−208.

(5) Kagan, C. R.; Lifshitz, E.; Sargent, E. H.; Talapin, D. V. Building Devices from Colloidal Quantum Dots. *Science* **2016**, *353*, No. aac5523.

(6) de Arquer, F. P. G.; Talapin, D. V.; Klimov, V. I.; Arakawa, Y.; Bayer, M.; Sargent, E. H. Semiconductor Quantum Dots: Technological Progress and Future Challenges. *Science* **2021**, *373*, No. eaaz8541.

(7) Kovalenko, M. V.; Protesescu, L.; Bodnarchuk, M. I. Properties and Potential Optoelectronic Applications of Lead Halide Perovskite Nanocrystals. *Science* **2017**, *358*, 745−750.

(8) Shyamal, S.; Pradhan, N. Nanostructured Metal Chalcohalide Photocatalysts: Crystal Structures, Synthesis, and Applications. *ACS Energy Lett.* **2023**, *8*, 3902−3926.

(9) Zhang, H.; Xia, Y.; Zhang, Y.; Ghorpade, U. V.; He, M.; Shin, S. W.; Hao, X.; Suryawanshi, M. P. The Rise of Chalcohalide Solar Cells: Comprehensive Insights From Materials to Devices. *Adv. Sci.* **2025**, *12*, No. 2413131.

(10) Palazon, F. Metal Chalcohalides: Next Generation Photovoltaic Materials? *Sol. RRL* **2022**, *6*, No. 2100829.

(11) Grandhi, G. K.; Hardy, D.; Krishnaiah, M.; Vargas, B.; Al-Anesi, B.; Suryawanshi, M. P.; Solis-Ibarra, S.; Gao, F.; Hoye, R. L. Z.; Vivo, P. Wide-Bandgap Perovskite-Inspired Materials: Defect-Driven Challenges for High-Performance Optoelectronics. *Adv. Funct. Mater.* **2024**, *34*, No. 2307441.

(12) Ghorpade, U. V.; Suryawanshi, M. P.; Green, M. A.; Wu, T.; Hao, X.; Ryan, K. M. Emerging Chalcohalide Materials for Energy Applications. *Chem. Rev.* **2023**, *123*, 327−378.

(13) He, J.; Hu, X.; Liu, Z.; Chen, W.; Longo, G. Prospect for Bismuth/Antimony Chalcohalides-Based Solar Cells. *Adv. Funct. Mater.* **2023**, *33*, No. 2306075.
(14) Li, J.; Han, S. S.; Guo, S. P. Chalcohalides: A Rising Type of Second-Order Nonlinear Optical Materials. *Eur. J. Inorg. Chem.* **2022**, *2022*, No. e202200419.
(15) Toso, S.; Akkerman, Q. A.; Martín-García, B.; Prato, M.; Zito, J.; Infante, I.; Dang, Z.; Moliterni, A.; Giannini, C.; Bladt, E.; Lobato, I.; Ramade, J.; Bals, S.; Buha, J.; Spirito, D.; Mugnaioli, E.; Gemmi, M.; Manna, L. Nanocrystals of Lead Chalcohalides: A Series of Kinetically Trapped Metastable Nanostructures. *J. Am. Chem. Soc.* **2020**, *142*, 10198−10211.
(16) Roth, A. N.; Opare-Addo, J.; Gi, E.; Mena, S.; Guirado, G.; Schaller, R. D.; Smith, E. A.; Vela, J. Solution-Phase Synthesis and Photoluminescence of Quaternary Chalcohalide Semiconductors. *Chem. Mater.* **2023**, *35*, 2165−2172.
(17) Roth, A. N.; Chen, Y.; Santhiran, A.; Opare-Addo, J.; Gi, E.; Smith, E. A.; Rossini, A. J.; Vela, J. Designing Complex $Pb_3SBr_xI_{4-x}$ Chalcohalides: Tunable Emission Semiconductors through Halide Mixing. *Chem. Sci.* **2023**, *14*, 12331−12338.
(18) Roth, A. N.; Porter, A. P.; Horger, S.; Ochoa-Romero, K.; Guirado, G.; Rossini, A. J.; Vela, J. Lead-Free Semiconductors: Phase-Evolution and Superior Stability of Multinary Tin Chalcohalides. *Chem. Mater.* **2024**, *36*, 4542−4552.
(19) Imran, M.; Caligiuri, V.; Wang, M.; Goldoni, L.; Prato, M.; Krahne, R.; De Trizio, L.; Manna, L. Benzoyl Halides as Alternative Precursors for the Colloidal Synthesis of Lead-Based Halide Perovskite Nanocrystals. *J. Am. Chem. Soc.* **2018**, *140*, 2656−2664.
(20) Creutz, S. E.; Crites, E. N.; De Siena, M. C.; Gamelin, D. R. Anion Exchange in Cesium Lead Halide Perovskite Nanocrystals and Thin Films Using Trimethylsilyl Halide Reagents. *Chem. Mater.* **2018**, *30*, 4887−4891.
(21) Creutz, S. E.; Crites, E. N.; De Siena, M. C.; Gamelin, D. R. Colloidal Nanocrystals of Lead-Free Double-Perovskites (Elpasolite) Semiconductors: Synthesis and Anion Exchange to Access New Materials. *Nano Lett.* **2018**, *18*, 1118−1123.
(22) Lin, C.-C.; Tan, S. J.; Vela, J. Chalcogenide and Pnictide Nanocrystals from the Silylative Deoxygenation of Metal Oxides. *J. Mater. Chem. A* **2017**, *5*, 20351−20358.
(23) Quarta, D.; Toso, S.; Giannuzzi, R.; Caliandro, R.; Moliterni, A.; Saleh, G.; Capodilup, A. L.; Debellis, D.; Prato, M.; Nobile, C.; Maiorano, V.; Infante, I.; Gigli, G.; Giannini, C.; Manna, L.; Giansante, C. Colloidal Bismuth Chalcohalide Nanocrystals. *Angew. Chem., Int. Ed.* **2022**, *61*, No. e202201747.
(24) Wechwithayakhlung, C.; Packwood, D. M.; Chaopaknam, J.; Worakajit, P.; Ittisanronnachai, S.; Chanlek, N.; Promarak, V.; Kongpatpanich, K.; Harding, D. J.; Pattanasattayavong, P. Tin(II) Thiocyanate $Sn(SCN)_2$ − A Wide Band Gap Coordination Polymer Semiconductor with a 2D Structure. *J. Mater. Chem. C* **2019**, *7*, 3452−3462.
(25) Castro-Méndez, A.-F.; Jahanbakhshi, F.; LaFollete, D. K.; Lawrie, B. J.; Li, R.; Perini, C. A. R.; Rappe, A. M.; Correa-Baena, J.-P. Tailoring Interface Energies via Phosphonic Acids to Grow and Stabilize Cubic $FAPbI_3$ Deposited by Thermal Evaporation. *J. Am. Chem. Soc.* **2024**, *146*, 18459−18469.
(26) Sharma, S.; Perini, C. A. R.; Brea, C.; Wieghold, S.; Li, R.; Dou, L.; Facchetti, A.; Hu, G.; Correa-Baena, J.-P. Bulky Cation-Modified Interfaces for Thermally Stable Lead Halide Perovskite Solar Cells. *Chem. Mater.* **2025**, *37*, 3676−3684.
(27) Putz, H.; Brandenburg, K. *Match! Version 3.11.5.203 (64-bit)*; Crystal Impact: Bonn, Germany, 2021 https://www.crystalimpact.de/match.
(28) Viezbicke, B. D.; Patel, S.; Davis, B. E.; Birnie, D. P. Evaluation of the Tauc Method for Optical Absorption Edge Determination: ZnO Thin Films as a Model System. *Phys. Status Solidi B* **2015**, *252*, 1700−1710.
(29) Harris, R. K.; Becker, E. D.; de Menezes, S. M. C.; Goodfellow, R.; Granger, P. Pure NMR nomenclature. Nuclear Spin Properties and Conventions for Chemical Shifts (IUPAC Recommendations 2001). *Appl. Chem.* **2001**, *73*, 1795−1818.
(30) Kresse, G.; Furthmuller, J. Efficiency of *Ab-initio* Total Energy Calculations for Metals and Semiconductors Using a Plane-Wave Basis Set. *Comput. Mater. Sci.* **1996**, *6*, 15−50.
(31) Jepsen, O.; Burkhardt, A.; Andersen, O. K. The Program TB-LMTO-ASA, version 4.7; Max-Planck-Institut fur Festkorperforschung: Stuttgart, Germany. 1999.
(32) Momma, K.; Izumi, F. VESTA 3 for Three-Dimensional Visualization of Crystal, Volumetric and Morphology Data. *J. Appl. Crystallogr.* **2011**, *44*, 1272−1276.
(33) Quarta, D.; Toso, S.; Saleh, G.; Caliandro, R.; Moliterni, A.; Griesi, A.; Divitini, G.; Infante, I.; Gigli, G.; Giannini, C.; Manna, L.; Giansante, C. Mixed Valence of Bismuth in Hexagonal Chalcohalide Nanocrystals. *Chem. Mater.* **2023**, *35*, 1029−1036.
(34) Quarta, D.; Toso, S.; Fieramosca, A.; Dominici, L.; Caliandro, R.; Moliterni, A.; Tobaldi, D. M.; Saleh, G.; Gushchina, I.; Brescia, R.; Prato, M.; Infante, I.; Cola, A.; Giannini, C.; Manna, L.; Gigli, G.; Giansante, C. Direct Band Gap Chalcohalide Semiconductors: Quaternary $AgBiSCl_2$ Nanocrystals. *Chem. Mater.* **2023**, *35*, 9900−9906.
(35) Haynes, W. M.; Lide, D. R.; Bruno, T. J. *CRC Handbook of Chemistry and Physics*, 103rd ed.; CRC Press: Boca Raton, Fl, 2022.
(36) Beecher, A. N.; Yang, X.; Palmer, J. H.; LaGrassa, A. L.; Juhas, P.; Billinge, S. J. L.; Owen, J. S. Atomic Structures and Gram Scale Synthesis of Three Tetrahedral Quantum Dots. *J. Am. Chem. Soc.* **2014**, *136*, 10645−10653.
(37) Schrems, M.; Ebner, G.; Liebner, F.; Becker, E.; Potthast, A.; Rosenau, T. Side Reactions in the System Cellulose/1-Alkyl-3-methylimidazolium Ionic Liquid. In *Cellulose Solvents: For Analysis, Shaping, and Chemical Modification*; Liebert, T. F.; Heinze, T. J.; Edgar, K. J., Eds.; American Chemical Society, 2010; Vol. *1033*, pp 149−164 DOI: 10.1021/bk-2010-1033.ch008.
(38) Mistewicz, K.; Das, T. K.; Nowacki, B.; Smalcerz, A.; Kim, H. J.; Hajra, S.; Godzierz, M.; Masiuchok, O. Bismuth Sulfoiodide (BiSI) Nanorods: Synthesis, Characterization, and Photodetector Application. *Sci. Rep.* **2023**, *13*, No. 8800.
(39) Tamilselvan, M.; Bhattacharyya, A. J. Antimony sulphoiodide (SbSI), a Narrow Band-Gap Non-Oxide Ternary Semiconductor with Efficient Photocatalytic Activity. *RSC Adv.* **2016**, *6*, 105980−105987.
(40) Cho, I.; Min, B.; Joo, S. W.; Sohn, Y. One-Dimensional Single Crystalline Antimony Sulfur Iodide, SbSI. *Mater. Lett.* **2012**, *86*, 132−135.
(41) Sadurni, M. D.; Timmo, K.; Mikli, V.; Volobujeva, O.; Mengu, I.; Krustok, J.; Grossverg-Kuusk, M.; Kauk-Kuusik, M. Preparation and Characterization of SbSeI Thin Films. *J. Sci.: Adv. Mater. Devices* **2024**, *9*, No. 100664.
(42) Jung, K.-W.; Choi, Y. C. Compositional Engineering of Antimony Chalcoiodides via a Two-Step Solution Process for Solar Cell Applications. *ACS Appl. Energy Mater.* **2022**, *5*, 5348−5355.
(43) Wibowo, A. C.; Malliakas, C. D.; Liu, Z.; Peters, J. A.; Sebastian, M.; Chung, D. Y.; Wessels, B. W.; Kanatzidis, M. G. Photoconductivity in the Chalcohalide Semiconductor, SbSeI: a New Candidate for Hard Radiation Detection. *Inorg. Chem.* **2013**, *52*, 7045−7050.
(44) Ran, Z.; Wang, X.; Li, Y.; Yang, D.; Zhao, X.-G.; Biswas, K.; Singh, D. J.; Zhang, L. Bismuth and Antimony-based Oxyhalides and Chalcohalides as Potential Optoelectronic Materials. *npj Comput. Mater.* **2018**, *4*, No. 14.
(45) Smith, M. D.; Connor, B. A.; Karunadasa, H. I. Tuning the Luminescence of Layered Halide Perovskites. *Chem. Rev.* **2019**, *119*, 3104−3139.
(46) Protesescu, L.; Yakunin, S.; Bodnarchuk, M. I.; Krieg, F.; Caputo, R.; Hendon, C. H.; Yang, R. X.; Walsh, A.; Kovalenko, M. V. Nanocrystals of Cesium Lead Halide Perovskites ($CsPbX_3$, X = Cl, Br, and I): Novel Optoelectronic Materials Showing Bright Emission with Wide Color Gamut. *Nano Lett.* **2015**, *15*, 3692−3696.

(47) Rosales, B. A.; Men, L.; Cady, S. D.; Hanrahan, M. P.; Rossini, A. J.; Vela, J. Persistent Dopants and Phase Segregation in Organolead Mixed-Halide Perovskites. *Chem. Mater.* **2016**, *28*, 6848−6859.
(48) Nie, R.; Im, J.; Seok, S. I. Efficient Solar Cells Employing Light-Harvesting $Sb_{0.67}Bi_{0.33}SI$. *Adv. Mater.* **2019**, *31*, No. 1808344.
(49) Groom, R. A.; Jacobs, A.; Cepeda, M.; Drummey, R.; Latturner, S. E. Structural and Optical Properties of Sb-Substituted BiSI Grown from Sulfur/Iodine Flux. *Inorg. Chem.* **2017**, *56*, 12362−12368.
(50) López-Paz, S. A.; Singh, H. K.; Méndez, A. S.; Multian, V.; Teyssier, J.; Aschauer, U.; Von Rohr, F. O. Tailoring Optical and Ferroelectric Properties in $Sb_{1-x}Bi_x$ SI van der Waals Chalcohalides towards Solar Absorber Applications. *J. Mater. Chem. A* **2026**, *14*, 1681−1690.
(51) Drake, G. A.; Keating, L. P.; Shim, M. Design Principles of Colloidal Nanorod Heterostructures. *Chem. Rev.* **2023**, *123*, 3761−3789.
(52) Beberwyck, B. J.; Surendranath, Y.; Alivisatos, A. P. Cation Exchange: A Versatile Tool for Nanomaterials Synthesis. *J. Phys. Chem. C* **2013**, *117*, 19759−19770.
(53) De Trizio, L.; Manna, L. Forging Colloidal Nanostructures via Cation Exchange Reactions. *Chem. Rev.* **2016**, *116*, 10852−10887.
(54) Wark, S. E.; Hsia, C.-H.; Son, D. H. Effects of Ion Solvation and Volume Change of Reaction on the Equilibrium and Morphology in Cation-Exchange Reaction of Nanocrystals. *J. Am. Chem. Soc.* **2008**, *130*, 9550−9555.
(55) Henkel, P.; Li, J.; Grandhi, G. K.; Vivo, P.; Rinke, P. Screening Mixed-Metal $Sn_2M(III)Ch_2X_3$ Chalcohalides for Photovoltaic Applications. *Chem. Mater.* **2023**, *35*, 7761−7769.
(56) Kikuchi, A.; Oka, Y.; Sawaguchi, E. Crystal Structure Determination of SbSI. *J. Phys. Soc. Jpn.* **1967**, *23*, 337−354.
(57) Pavel, M. R. S.; Chen, Y.; Santhiran, A.; Gi, E.; Ochoa-Romero, K.; Miller, G. J.; Guirado, G.; Rossini, A. J.; Vela, J. Coloring Tetrahedral Semiconductors: Synthesis and Photoluminescence Enhancement of Ternary II-III_2-VI_4 Colloidal Nanocrystals. *ACS Energy Lett.* **2024**, *9*, 5012−5018.
(58) Rosales, B. A.; White, M. A.; Vela, J. Solution-Grown Sodium Bismuth Dichalcogenides: Toward Earth-Abundant, Biocompatible Semiconductors. *J. Am. Chem. Soc.* **2018**, *140*, 3736−3742.
(59) Miller, G. J. The "Coloring Problem" in Solids: How It Affects Structure, Composition and Properties. *Eur. J. Inorg. Chem.* **1998**, *1998*, 523−536.
(60) Kavanagh, S. R.; Savory, C. N.; Scanlon, D. O.; Walsh, A. Hidden Spontaneous Polarisation in the Chalcohalide Photovoltaic Absorber $Sn_2SbS_2I_3$. *Mater. Horiz.* **2021**, *8*, 2709−2716.
(61) Nicolson, A.; Breternitz, J.; Kavanagh, S. R.; Tomm, Y.; Morita, K.; Squires, A. G.; Tovar, M.; Walsh, A.; Schorr, S.; Scanlon, D. O. Interplay of Static and Dynamic Disorder in the Mixed-Metal Chalcohalide $Sn_2SbS_2I_3$. *J. Am. Chem. Soc.* **2023**, *145*, 12509−12517.

https://doi.org/10.1021/acs.chemmater.5c02918
Chem. Mater. 2026, 38, 2755−2766